Acoustic Field of a Ballistic Shock Wave Therapy Device

3 authors:

Robin Olav Cleveland
University of Oxford
252 PUBLICATIONS **3,180** CITATIONS

Parag V Chitnis
George Mason University
82 PUBLICATIONS **218** CITATIONS

Scott R Mcclure
Iowa State University
66 PUBLICATIONS **1,019** CITATIONS

Some of the authors of this publication are also working on these related projects:

Project — Consequences of shock waves and unltrasound induced cavitation near lipid interfaces and its implications for drug delivery and neuromodulation View project

Project — Acousto-Optic Sensing and Imaging View project

ELSEVIER

doi:10.1016/j.ultrasmedbio.2007.02.014

● *Original Contribution*

ACOUSTIC FIELD OF A BALLISTIC SHOCK WAVE THERAPY DEVICE

ROBIN O. CLEVELAND,* PARAG V. CHITNIS,* and SCOTT R. McCLURE[†]
*Department of Aerospace and Mechanical Engineering, Boston University, Boston, MA, USA; and [†]Department of
Veterinary Clinical Sciences, College of Veterinary Medicine, Iowa State University, Ames, IA, USA

Abstract—Shock wave therapy (SWT) refers to the use of focused shock waves for treatment of musculoskeletal indications including plantar fasciitis and dystrophic mineralization of tendons and joint capsules. Measurements were made of a SWT device that uses a ballistic source. The ballistic source consists of a handpiece within which compressed air (1–4 bar) is used to fire a projectile that strikes a metal applicator placed on the skin. The projectile generates stress waves in the applicator that transmit as pressure waves into tissue. The acoustic fields from two applicators were measured: one applicator was 15 mm in diameter and the surface slightly convex and the second was 12 mm in diameter the surface was concave. Measurements were made in a water tank and both applicators generated a similar pressure pulse consisting of a rectangular positive phase (4 μs duration and up to 8 MPa peak pressure) followed by a predominantly negative tail (duration of 20 μs and peak negative pressure of −6 MPa), with many oscillations. The rise times of the waveforms were around 1 μs and were shown to be too long for the pulses to be considered shock waves. Measurements of the field indicated that region of high pressure was restricted to the near-field (20–40 mm) of the source and was consistent with the Rayleigh distance. The measured acoustic field did not display focusing supported by calculations, which demonstrated that the radius of curvature of the concave surface was too large to effect a focusing gain. Other SWT devices use electrohydraulic, electromagnetic and piezoelectric sources that do result in focused shock waves. This difference in the acoustic fields means there is potentially a significant mechanistic difference between a ballistic source and other SWT devices. (E-mail: robinc@bu.edu)   © 2007 World Federation for Ultrasound in Medicine & Biology.

Key Words: Shock wave therapy, Ballistic pressure source, Therapeutic ultrasound.

INTRODUCTION

Shock wave therapy (SWT) has emerged as a viable technology for treating orthopedic abnormalities such as nonunion of bones, plantar fasciitis, heel spur, tennis elbow and calcification on bones (Ogden et al. 2001). SWT devices use short acoustic pulses that are focused on the specific anatomical location of the problem. The mechanism of action is not fully understood, but it appears that shock waves can induce both an analgesic effect (Ohtori et al. 2001; Takahashi et al. 2003) and tissue repair processes (Wang et al. 2002, 2003). The promise of SWT has been tempered by reports showing no improvement over placebo (Buchbinder et al. 2002; Haake et al. 2002). The use of SWT in veterinary medicine has mirrored human applications. Tendon and ligament injuries (Kersh et al. 2004; McClure et al. 2004),

as well as stress fractures (McClure et al. 2004) and osteoarthritis (Dahlberg et al. 2005), have been evaluated in controlled studies and are routinely used in clinical cases. However, results in veterinary applications are also not always consistent, *e.g.*, SWT of equine lameness resulted in no improvement in one study (Brown et al. 2005) but a statistically significant decrease in another study (Dahlberg et al. 2006). The origin for conflicting data, in both the clinical and veterinary literature, is likely related to a poor understanding of the mechanisms and lack of guidance about the appropriate settings on the various devices on the market.

The technology to create the pulses in SWT has in general been derived from shock wave lithotripters (used to fragment kidney stones) in particular: electrohydraulic (EH), electromagnetic (EM) and piezoelectric (PE) sources that have been developed by lithotripter manufacturers have been transitioned into SWT. The characterization of the fields of EH, EM and PE sources has been reported widely in the lithotripsy community. One source used in SWT, which does not have its roots in

Address correspondence to: Dr. Robin O. Cleveland, Address: Department of Aerospace and Mechanical Engineering, Boston University, 110 Cummington St., Boston, MA 02215. E-mail: robinc@bu.edu
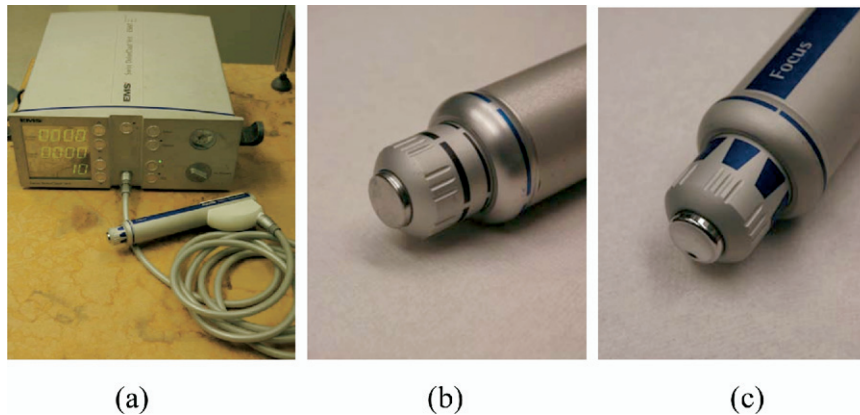
Fig. 1. (a) The entire SWT system of an EMS Swiss Dolorclast Vet (Electro Medical Systems) excluding the air compressor. (b) The 15-mm diameter convex "unfocused" applicator. (c) The 12-mm diameter concave "focused" applicator.

lithotripsy, is the ballistic source in which stress waves are generated by means of a projectile impacting a solid surface. The principle is identical to that used by pneumatic jack-hammers (Pang and Goldsmith 2005) and the Hopkinson bar that is used in the materials testing community (Hopkinson 1914; Gama et al. 2004). We are unaware of pressure measurements being reported in the peer-reviewed literature. In this manuscript we present measurements of the acoustic field of a SWT device that uses a ballistic source, and we attempt to address some issue with the nomenclature attached to the source.

MATERIALS AND METHODS

Experimental apparatus

Measurements were carried out on an EMS Swiss Dolorclast Vet (Electro Medical Systems, Nyon, Switzerland). This is a veterinary version of the EMS Swiss Dolorclast used for orthopaedic pain therapy in humans. A photograph of the control unit and the handpiece of this system is shown in Fig. 1a; not shown is the air compressor that provides the compressed gas needed to launch the projectile. Different types of applicators can be attached to the handpiece. In these experiments two types of applicators were use: one, referred to as unfocused, was a convex shaped applicator with a 15-mm diameter (Fig. 1b) and the second, referred to as focused, was a concave applicator with a 12-mm diameter (Fig. 1c). The pressure used to drive the projectile could be varied continuously from 0 bar to 4 bar using a dial on the front panel (1 bar = 10^5 Pa). In what follows, the driving pressure is referred to as the "pressure setting" and will be given in bar to be consistent with the dial on the device.

Acoustic measurements of the pressure field were conducted in a water tank (30 cm long × 25 cm deep × 20 cm wide). Pressure waves from the Dolorclast (Electro Medical Systems) were transmitted into the tank through a membrane cut from an overhead transparency (approximately 100 μm thick and 20 mm in diameter) that was fitted to a port in the side of the tank. Using a three medium analysis (Blackstock 2000), the pressure transmission coefficient of the membrane was calculated to be >95% for frequencies <1 MHz and 80% at 2 MHz. For the measurements reported below, signal level was <1% of the peak for frequencies above 2 MHz, and so the membrane should have a negligible effect on the pressure waves. The face of the applicator was covered with coupling gel (ESWT contact gel, Electro Medical Systems) and then fixed rigidly in contact with the membrane. Care was taken to ensure there were no bubbles in the coupling gel—this could be done visually because the membrane was transparent. Within the tank, the nearest interfaces (walls or surface) to the applicator were more than 100 mm away (approximately 300 μs round trip) to ensure that these reflections did not interfere with the pressure field being measured.

The pressure was measured with a polyvinylidene fluoride (PVDF) "capsule" hydrophone (HGL-0200 OndaCorp, Sunnyvale, CA, USA) with a 20-dB in-line preamplifier (AH2010, OndaCorp). The hydrophone has an active element that is nominally 200 μm in diameter and a published bandwidth of 0.2 to 40 MHz. The signal was recorded on a digital storage scope and transferred to computer for analysis. Acoustic parameters were calculated based on the International Electrotechnical Commission (IEC) standard for shock wave lithotripsy (IEC 1998) The transducer was mounted to a 3-D motorized stage (nominal step of 5 μm), which allowed computer-controlled scanning of the acoustic field. The hydrophone was moved at 0.5-mm intervals in the lateral

direction and 1-mm intervals in the axial direction. The hydrophone was moved at a speed of approximately 1 mm/s, and at the end of each step the computer paused for 2 s to ensure the hydrophone was at rest.

Theory

We briefly cover some acoustic theory that covers aspects of diffracting beams and nonlinear distortion, which will be relevant to the measurements that are reported later.

The acoustic field of a piston radiator is commonly divided into the near-field (where the sound is nominally collimated) and the far-field (where the sound is spherically spreading). The Rayleigh distance R_D is one metric for defining the transition between the near and far-field and, for a circular source, is given by:

$$R_D = \frac{1}{2}ka^2 \tag{1}$$

where the wavenumber $k = 2\pi f/c_0$, f is the frequency, c_0 the speed of sound and *a* the radius of the source (Blackstock 2000).

Focusing of sound waves can be achieved by changing the curvature of the radiating surface, adding a lens, or electronically beamforming an array. In each case, for a spherically focused wave, the pressure gain G as a result of focusing is given by:

$$G = R_D/F_L \tag{2}$$

where F_L is the geometrical focal length (Szabo 2004). Inspection of eqn (2) shows that for focusing to effect a gain greater than unity, it is necessary that the Rayleigh distance be longer than the focal length.

A shock wave consists of a very abrupt transition in pressure (and other acoustic field variables) in both time and space. The thickness of the transition is governed by the interaction of nonlinear distortion and absorption. When these two effects are in balance in a thermoviscous fluid (such as water) then the shape of the shock is given by the Taylor shock profile (Blackstock et al. 1998). The rise time t_{RT} of the Taylor shock profile (time for the pressure to change from 10% of the peak pressure to 90% of the peak pressure) is given by:

$$t_{RT} = \frac{4.4\rho_0\delta}{\beta\Delta P} \tag{3}$$

where ρ_0 is density, δ is the diffusivity of sound (thermal and viscous losses), β the coefficient of nonlinearity and ΔP the pressure jump of the shock. For a 1-MPa shock in water ($\rho_0 = 1000$ kg/m^3, $\delta = 1.7 \times 10^{-4}$ m^2/s and $\beta = 3.5$), the Taylor shock thickness is 0.2 ns. The finite bandwidth of the transducer used here (40 MHz) prevents a shock front of such a short duration having the correct rise time. However, a simulation of the step response of the transducer transfer function resulted in a predicted rise time of 9 ns and therefore the rise time of a steady-state 1-MPa shock will appear to have a rise time of 9 ns.

If a waveform does not initially contain a shock then as it propagates it can develop a shock by the process of nonlinear distortion. The plane wave shock formation distance is the distance that a plane wave needs to propagate in a lossless fluid such that nonlinear distortion results in an infinite slope (discontinuity) in the wave and is given by (Blackstock et al. 1998)

$$\bar{x} = \frac{\rho_0 c_0^3}{\beta \max(\partial p/\partial t)} \tag{4}$$

where $\max(\partial p/\partial t)$ is the maximum value of the time derivative of the pressure. Note the inverse relationship to the derivative of the pressure waveform means that a smooth waveform requires a long propagation distance to form a shock. For a spherical spreading wave, the shock formation distance is modified (Blackstock et al. 1998) to the following expression

$$\bar{r} = r_0 \exp(\bar{x}/r_0) \tag{5}$$

where r_0 is the radial distance where $\max(\partial p/\partial t)$ was measured and $\bar{r}$ is the radial distance where a shock will form. The shock formation distance for a spherically spreading wave is always longer than that of a plane wave because the spreading reduces the amplitude of the wave, which in turn results in weaker nonlinear distortion.

RESULTS

Unfocused applicator

The unfocussed applicator had a diameter of 15 mm and was slightly convex, with the centre of the applicator extending approximately 0.7 mm from the edge (effective radius of curvature of 41 mm). For this applicator the pressure waveform, at a range of 10 mm from the applicator, for a setting of 3.0 bar is shown in Fig. 2a. The waveform consists of a leading positive phase with a peak positive pressure p+ of 5.6 MPa and a duration (based on the time the pressure exceeds p+/2) of 3.8 μs. The subsequent negative phase quickly reaches a peak negative pressure p− of −9.2 MPa and then relaxes, with a notable amount of internal structure, to baseline after approximately 15 μs. The structure in the tail was not a result of reverberation between the applicator and hydrophone. For this measurement the separation distance was such that the reverberation signal should arrive at 16 μs, and for larger separation distances the coda remained similar (example shown below). It is likely that
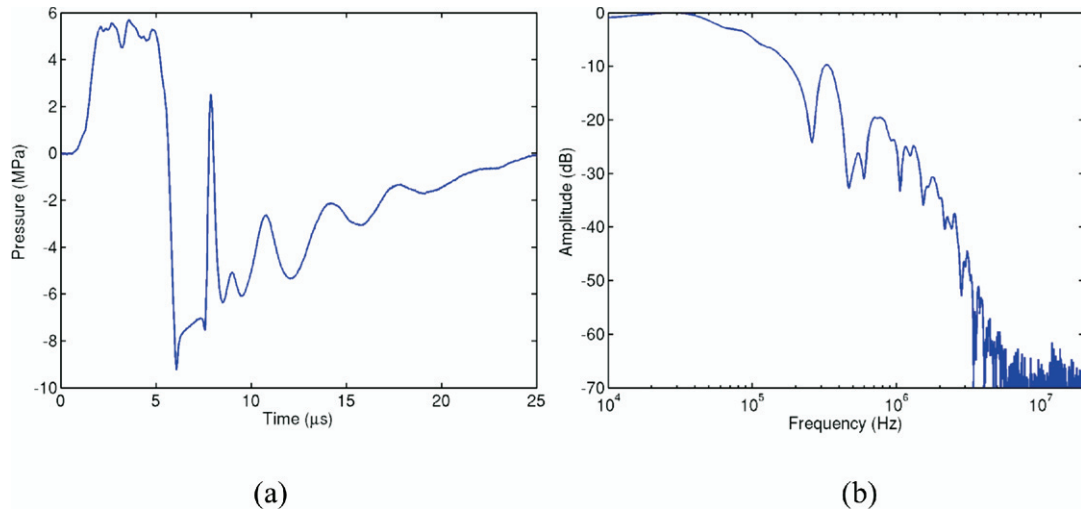
Fig. 2. (a) The measured pressure waveform plotted *vs.* time for the unfocused applicator operated at 3 bar at a distance of 10 mm. (b) The amplitude spectrum as a function of frequency.

the coda is a combination of reverberation of stress waves in the applicator and the arrival of the edge wave from the applicator. At a distance of 10 mm, the edge wave would be expected to arrive at 8 μs and, based on the geometry of the applicator, the time difference between a compressional wave that goes through the applicator and a shear wave that reflects from the side of the applicator is about the same. The energy flux density (IEC 1998) was calculated by integrating the intensity to 25 μs (waveform displayed in Fig. 2a) and produced a value of 0.234 mJ/mm^2.

The spectrum of the wave is shown in Fig. 2b and the energy is predominantly below 100 kHz. In this region the low frequency response of the hydrophone will be affected by the bandwidth of the electronics and diffraction by the hydrophone. Determining the effect of diffraction is beyond the scope of this manuscript; however, the electronics can be modeled as low-pass filter with a -3 dB frequency of 10 kHz. The effect of this filtering is shown in Fig. 3. The response of the filter to a 4-μs-long step input is shown and it can be seen that the resulting waveform is affected by the response of the electronics. Figure 3 also shows a waveform measured at 15 mm to which an inverse Weiner filter was implemented to deconvolve the response of the electronics from the measured waveform. It can be seen that the deconvolution process alters neither the shape of leading pressure rise nor the peak positive or negative pressures. Note that for this separation the edge wave should arrive at 11 μs and the reverberation at 20 μs. This is further evidence that the structure of the coda is mainly the result of reverberation in the applicator.

Because the waveform is a broadband pulse it does not have a unique Rayleigh distance. The range for the near to far-field transition can be estimated based on characteristic features of the wave. If the leading positive phase was modeled as part of a wave with a fundamental period of 7.8 μs then the corresponding frequency is around 130 kHz, which has a Rayleigh distance of 15 mm. From the spectrum, a peak can be observed at 330 kHz with a corresponding Rayleigh distance of 39 mm. Therefore, the transition to spherical spreading will likely occur in this range.

The spatial distribution of the peak positive and negative pressure is displayed in Fig. 4a and b, respectively. It can be observed that there is a monotonic decay
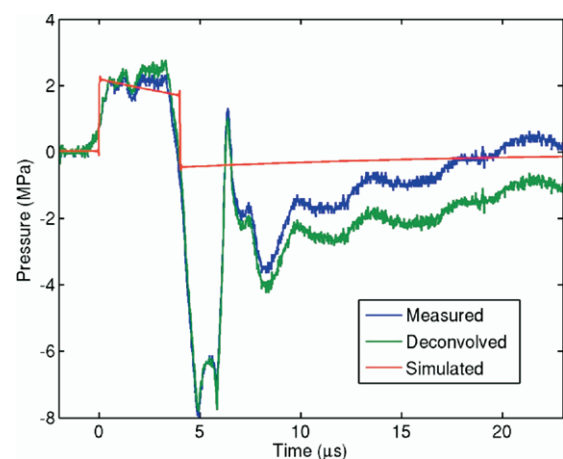

Fig. 3. The effect of the hydrophone transfer function on the measured waveforms. The blue line shows the raw measured waveform and the green line the waveform after deconvolving the transfer function of the in-line amplifier. The red line shows a simulation of the response of the amplifier to a top-hat input waveform.
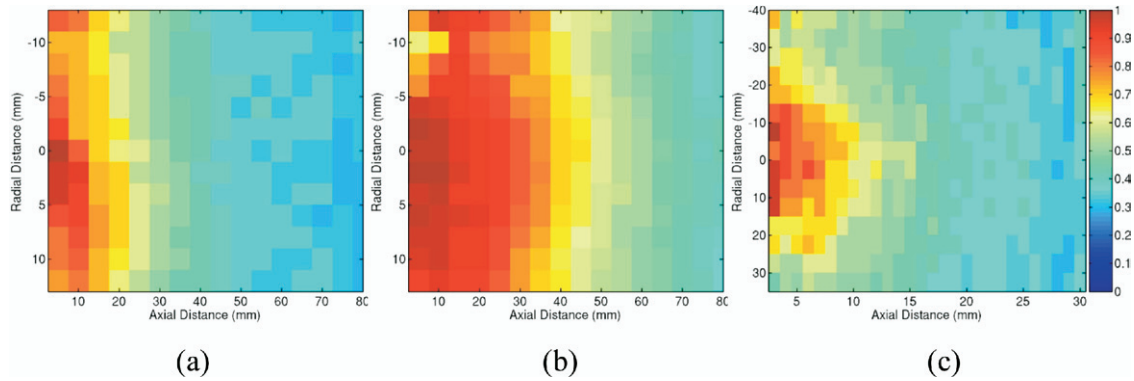
Fig. 4. The spatial distribution of the pressure field, as a function of radial distance and axial distance, for the focused applicator operated at 3.5 bar. (a) Map of p+. The pressure scale is from 0 to 3.5 MPa. (b) Map of p−. The pressure scale is from 0 to −8 MPa. (c) Map of p+ in the plane normal to that shown in (a) and for a reduced axial range (30 mm). The pressure scale is from 0 to 3 MPa. The nearest measurement to the applicator was at a range of 3 mm. The images show that the region of maximum pressure is localized to the source and is about as wide as the applicator.

with distance from the source. The decay approaches 1/r spherical spreading for distances greater than 20 mm— consistent with the estimated Rayleigh distance. The "focal" region was defined in terms of the −6 dB amplitude region, *i.e.*, a region demarcated by the isobar of half the peak pressure. In this case the −6 dB region is restricted to a distance of 40 mm for the peak positive pressure and so the transducer can be modeled to first order as consisting of a plane wave for the first 20 mm followed by spherical spreading with an $r_0 = 20$ mm. For the peak negative pressure, the −6 dB distance was approximately 60 mm. Figure 4c shows a plot in the orthogonal plane over a larger spatial area, showing that the field is symmetric and also that the lateral extent of the field is limited essentially to the diameter of the transducer as one would expect for the near-field of a piston transducer.

Figure 5 shows the variation in peak positive and negative pressure, measured 10 mm from the surface of the applicator, as a function of pressure setting for steps of 0.5 bar. There was an initial monotonic increase in p+ and p−, followed by an apparent saturation for settings of 3 bar and above. In no case was a shock wave measured. The maximum measured amplitude of the leading positive pulse was 7 MPa, which has a theoretical Taylor shock rise time of 0.02 ns. Because of the finite bandwidth of the hydrophone, this rise time would be measured as 9 ns. The measured rise time of the leading edge was 800 ns, which is 90 times longer than would be expected for a shock wave. Therefore, at a distance of 10 mm the waveform has not yet evolved into a shock wave. The maximum slope of the wavefront was 8.75 MPa/μs, which, based on eqn (4), results in a plane wave shock formation distance of 110 mm. However, because the wave is spherically spreading beyond 40 mm, the shock formation distance (eqn (5)) becomes

49 m, much larger than the propagation distance in humans or equines. We note that use of 40 mm gives the most conservative estimate of the shock formation distance; if a smaller value is used then the effects of spherical spreading are more pronounced and the shock formation becomes longer. We also note that the absorption in tissue is of the order 0.3 dB/cm at 1 MHz. Assuming absorption varies linearly with frequency, this corresponds to 0.03 dB/cm at 100 kHz. Therefore, propagation through 49 m of tissue would result in 147 dB of amplitude reduction, which would mean the wave will have been attenuated before a shock can form. The measurements indicate that the source does not generate a shock wave and that there is not enough nonlinearity to produce a shock wave.
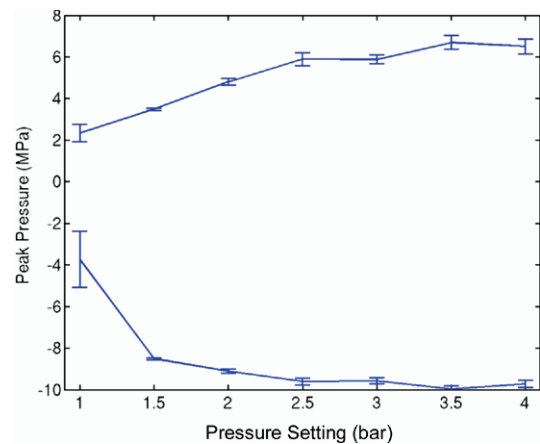

Fig. 5. The variation of peak pressure measured 10 mm from the face of the unfocused applicator as a function of pressure setting. The mean and standard deviation of 20 measurements are shown. Both p+ and p− appear to saturate for pressure settings of 2.5 bar and more.
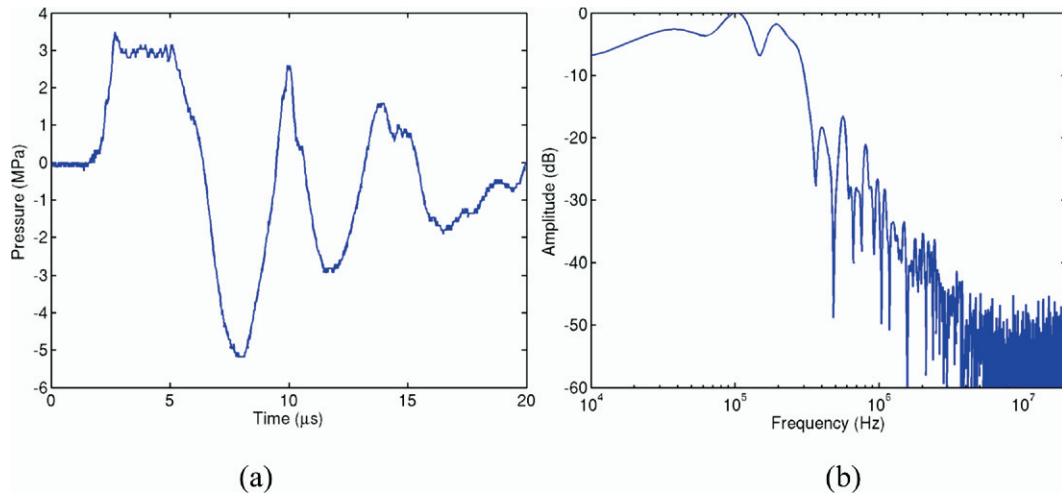
(a)   (b)

Fig. 6. (a) The measured pressure waveform plotted *vs.* time for the focused applicator operated at 3 bar at a distance of 10 mm. (b) The amplitude spectrum as a function of frequency.

Focused applicator

The focused applicator had a diameter of approximately 12 mm and was concave. The maximum depth of the cavity was 0.18 mm, corresponding to a radius of curvature of about 100 mm. Based on the speed of longitudinal waves in steel (6100 m/s) and water (1500 m/s), this curvature should result in a geometrical focus of 133 mm. A representative waveform, measured at a range of 10 mm from the focused applicator for a pressure setting of 3.0 bar, is shown in Fig. 6a. The waveform has a similar structure to that of the unfocused applicator shown in Fig. 2: a leading positive phase, followed by a negative tail with some spikes. For the focused applica-

tor, the leading positive phase has a peak pressure of 3.4 MPa and a duration of 3.4 μs. The tensile phase of the waveform has a peak amplitude of -5.2 MPa and is followed by a complex tail. The energy flux density was 0.158 mJ/mm^2. The spectra (Fig. 6b) is similar to that measured by the unfocused applicator in that the energy is principally below 100 kHz; however the structure above 100 kHz does show some differences.

The spatial distribution of the peak positive and negative pressures for the focused applicator for a pressure setting of 3.5 bar are shown in Fig. 7a and b, respectively. The data show no indication of focusing—both the positive and negative pressures drop off
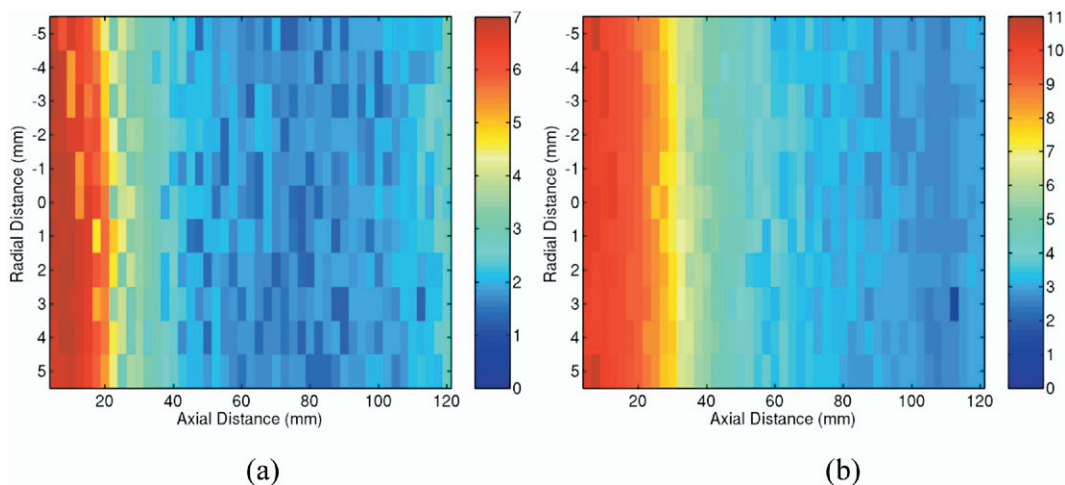

(a)   (b)

Fig. 7. The spatial distribution of (a) the peak positive pressure and (b) the peak negative pressure as a function of radial distance and axial distance for the focused applicator operated at 3.5 bar. Similar to that of Fig. 4, the maximum pressure is confined to a region near the applicator and there is no indication of focusing. The color bar is in MPa and the nearest measurement to the applicator was at a range of 3 mm.
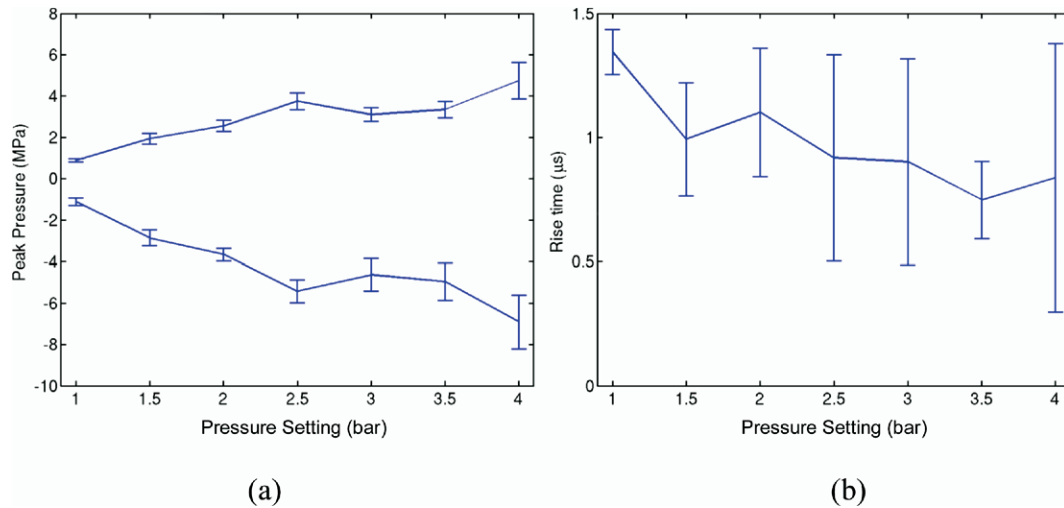
Fig. 8. (a) Peak positive and negative acoustic pressures *vs.* pressure setting for the focused applicator. (b) Rise time as a function of pressure setting. All of the rise times exceeded 0.5 μs and are too long to be considered shock waves for the measured peak positive pressure. Measurements were made 10 mm from the applicator.

monotonically with range from the transducer face. Based on the measurements, the effective distances where spherical spreading occurred was 15 mm for the peak positive pressure and 25 mm for the peak negative pressure; these are smaller than the unfocused applicator because the effective size of the focused applicator is smaller.

The dependence of the peak pressures with the pressure setting of the ballistic projectile is shown in Fig. 8a for measurements made at a distance of 10 mm from the applicator. There is a general increase in peak pressure with pressure setting; however, there is a small dip between 2.5 and 3.0 bar. We suspect this may have been the result of a degradation in the coupling between the hand piece and the membrane that connects to the tank—a topic considered in the next section.

None of the waveforms measured had a shock front. Figure 8b shows the rise time of the leading edge as a function of the pressure setting and it remains around 1 μs for all settings. The highest amplitude waveform had a peak pressure of 6 MPa and a rise time of 0.8 μs, which resulted in plane wave shock formation distance of 130 mm. When spherical spreading is taken into account, the shock formation distance is 80 km!

Pulse rate and coupling

The Dolorclast can be fired at pulse repetition rates as high as 15 Hz. Figure 9 shows the dependence of the peak pressures on pulse rate for a pressure setting of 3.5 bar with the focused applicator. It can be seen that the peak positive pressure was stable with pulse rate and the peak negative pressure showed an increase as high as 8 Hz, after which it was stable.

At the very highest pulse rate (15 Hz), there was a decrease in the peak positive pressure. Upon visual inspection it could be seen that bubbles were trapped in the coupling gel between the applicator and the membrane on the tank. It appeared that enough bubbles had accumulated in the gel to scatter the pressure wave before it entered the tank. Figure 10 shows a pressure waveform measured 10 mm from the face of the concave transducer after approximately 400 pulses had been fired, at which point a bubble (approx. 1 mm in diameter) could be observed in the gel between the applicator and the membrane. It can be seen that the waveform has been dramatically altered; when compared with Fig. 6a, the positive pressure is reduced and there is ringing in the tail,
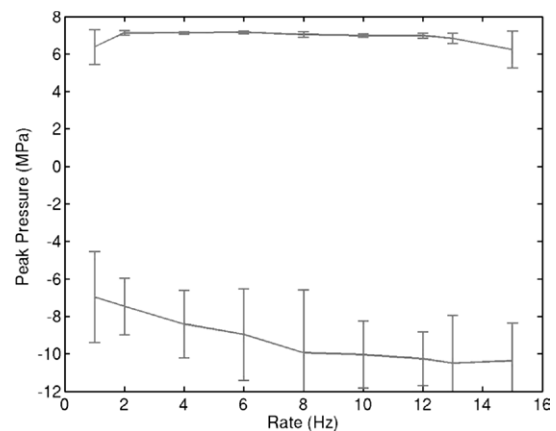

Fig. 9. The dependence of peak pressure on rate for the focused applicator operated at 3.5 bar. The peak positive pressure is quite stable with rate. The negative pressure initially increases and then saturates.
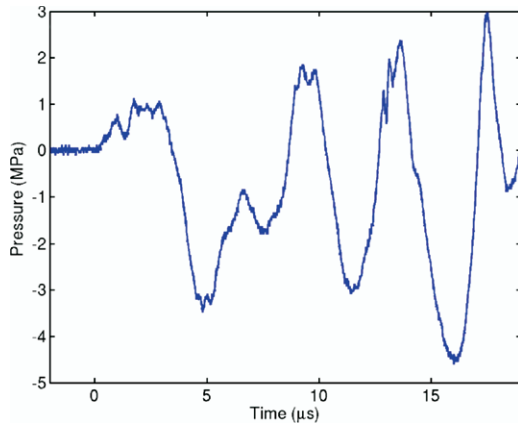
Fig. 10. A pressure waveform measuring 10 mm for the focused applicator operated at 3.0 bar after a visually detectable bubble developed in the coupling gel.

which is likely because of oscillations of the bubble or reverberation between the bubble and the applicator. The presence of bubbles in the gel was an issue with the concave applicator where the bubbles appeared to be trapped easily in the concave depression. For the unfocused applicator, the problem with bubbles in the gel was much less pronounced, presumably because the convex geometry of the surface, along with the pressure by which the therapy head is pushed against the membrane, resulted in bubbles being squeezed to the outer edges of the applicator.

DISCUSSION

The measurements reported here show that the ballistic source produces an acoustic pulse with peak pressure as high as 8 MPa. For both the focused and unfocused applicators, the waveform consisted of a leading positive phase with a duration around 4 μs. This was followed by a tail with lots of structure. The -6 dB region of the pressure field was not a cigar-shaped focal volume, as is typically found in other SWT devices, but rather a region of space that extended from the applicator surface to a distance of 40 mm for the unfocused applicator and 20 mm for the focused applicator. These distances were consistent with the predicted Rayleigh distance that bounds the near field of a piston source. The width of the region of a -6 dB pressure region was roughly the same as the diameter of the applicator, which is also consistent with the near field of a piston. We note that the Dolorclast (Electro Medical Systems) can also use a 6-mm convex applicator, for which the -6 dB pressure region will be reduced even further—theoretically to about 10 mm long and 6 mm wide. The concave applicator was found to not generate a focused field. Further, an analysis of the properties of the concave

applicator indicated that the apparent focal length is greater than the Rayleigh distance, and therefore the acoustic field would undergo spreading before the geometrical focal point, rendering focusing impossible.

The measurements made here indicated that the ballistic source did not generate shock waves. This was ascertained by measuring the rise time of the pressure pulses. For the peak pressures generated by the ballistic source, a steady-state shock would result in a rise time much shorter than is possible to measure, and the measured rise time should be limited by the response of the hydrophone ($\sim$10 ns). The measured rise time was of the order of 1 μs, which was too long for the pulse to be considered a shock wave. Further, analysis of the shock formation distance indicated that the nonlinear distortion was not strong enough to result in a shock front. We note that the measurements were made in water, which is an almost ideal homogeneous medium. In practice the shock waves are applied to targets in the body which are highly heterogeneous—in particular the presence of bone will result in a much more complex field. We anticipate that the presence of the heterogeneous medium will further reduce nonlinear effects from what were measured in water.

The measurements showed that the acoustic output was stable for pulse repetition rates from 1 to 15 Hz, but we found that at higher pulse rates, maintaining coupling was a challenge for the focused applicator in particular. The coupling could be monitored relatively easily during these *in-vitro* experiments because both the tank and membrane were optically clear. However, in a clinical treatment, monitoring of coupling cannot be carried out visually and therefore it is possible that pressure waves could be administered without the user being aware that the full amplitude of the pressure wave is not being delivered into the body. Coupling is an issue with all SWT devices, but is perhaps more challenging for the ballistic source because the motion of the projectile results in recoil of the handpiece with the potential for the applicator to disconnect from the skin. This is particularly an issue with the focused applicator where the concave shape could trap bubbles.

Although the ballistic source investigated marketed with both the terms "shock wave" and "focused," the device technically does not generate a focused shock wave. Electrohydraulic sources employ focusing by means of a reflector and generate shock waves at the spark source; for all settings the EH source results in a shock wave at the focus. Electromagnetic and piezoelectric sources also use focusing but do not generate shock waves at the source—they rely on nonlinear propagation distortion to produce a shock along the path to the focus. For mid and high-amplitude settings, the waveforms are shocked and the peak amplitudes and rise times are

comparable to those of the EH source—however, at low-amplitude settings the waveforms do not contain shocks (Coleman et al. 1991; Buizza et al. 1995). Thus for treatment protocols at low settings, the piezoelectric and electromagnetic sources will also not produce shock waves. The nomenclature of SWT therefore has a mismatch with the technical definition of a shock wave. Whether this is simply an issue of semantics or whether there is something specific about the shock front that is necessary for effective SWT cannot be ascertained until the mechanisms are better understood.

Our work did not assess the efficacy of the ballistic source in treating musculoskeletal indications. However, these measurements were motivated by conflicting reports on the impact of SWT on lameness in horses. In particular, the study that found no immediate pain relief used a ballistic source (Brown et al. 2005) and the successful study used an electrohydraulic source (Dahlberg et al. 2006). The marked difference in the acoustic fields of these sources could be the reason for the difference in outcomes.

REFERENCES

Blackstock DT. Fundamentals of Physical Acoustics. New York, NY: Wiley, 2000.

Blackstock DT, Hamilton MF, Pierce AD. Progressive waves in lossless and lossy fluids. In Hamilton MF, Blackstock DT, eds: Nonlinear Acoustics. Chestnut Hill, MA: Academic Press, 1998.

Brown KE, Nickels FA, Caron JP, Mullineaux DR, Clayton HM. Investigation of the immediate analgesic effects of extracorporeal shock wave therapy for treatment of navicular disease in horses. Vet Surg 2005;34:554–558.

Buchbinder R, Ptasznik R, Gordon J, Buchanan J, Prabaharan V, Forbes A. Ultrasound guided extracorporeal shock wave therapy for plantar fasciitis. JAMA 2002;288:1364–1372.

Buizza A, Dell'Aquila T, Giribona P, Spagno C. The performance of different pressure pulse generators for extracorporeal lithotripsy: A comparison based on commercial lithotripters for kidney stones. Ultrasound Med Biol 1995;21(2):259–272.

Coleman AJ, Choi MJ, Saunders JE. Influence of output setting on acoustic field of a shock wave lithotriptor. In Paumgartner G, Sauerbruch T, Sackmann M, et al, editors: Lithotripsy and Related Techniques for Gallstone Treatment. St. Louis, MO: Mosby–Year Book, 1991:1–6.

Dahlberg JA, Fitch G, Evans RB, McClure SR, Conzemius M. The evaluation of extracorporeal shockwave therapy in naturally occurring osteoarthritis of the stifle joint in dogs. Vet Comp Orthop Traumatol 2005;18:147–152.

Dahlberg JA, McClure SR, Evans RB, Reinerstein EL. Force platform evaluation of analgesia resulting from focused extracorporeal shock wave therapy in unilateral forelimb lameness. J Am Vet Med Assoc 2006;229(1):100–103.

Gama BA, Lopatnikov SL, Gillespie JW Jr. Hopkinson bar experimental technique: A critical review. Appl Mech Rev 2004;57:223–250.

Haake M, König IR, Decker T, Riedel C, Buch M, Müller H-H, Vogel M, Auersperg V, Maier-Boerries O, Betthäuser A, Fischer J, Loew M, Müller I, Rehak HC, Gerdesmeyer L, Maier M, Kanovsky W. Extracorporeal shock wave therapy in the treatment of lateral epicondylitis: A randomized multicenter trial. J Bone Joint Surg Am 2002;84:1982–1991.

Hopkinson B. A method of measuring the pressure produced in the detonation of high explosives or by the impact of bullets. Phil Trans Royal Soc London 1914;213:437–456.

International Electrotechnical Commission. IEC 61846 Ultrasonics–Pressure pulse lithotripters–Characteristics of fields. Geneva, Switerland: International Electrotechnical Commission, 1998.

Kersh KD, McClure SR, Evans RB, Moran L. Ultrasonographic evaluation of extracorporeal shock wave therapy on collagenase-induced superficial digital flexor tendonitis. Proc Am Assoc Equine Pract 2004;50:257–260.

McClure SR, VanSickle D, Evans RB, Reinerstein EL, Moran L. The effects of extracorporeal shock-wave therapy on the ultrasonographic and histologic appearance of collagenase-induced equine forelimb suspensory ligament desmitis. Ultrasound Med Biol 2004;30:461–467.

McClure SR, VanSickle D, White RM. Effects of extracorporeal shock wave therapy on bone. Vet Surg 2004;33:40–48.

Ogden JA, Alvarez RG, Levitt R, Marlow M. Shock wave therapy (Orthotripsy4) in musculoskeletal disorders. Clin Orthop Relat Res 2001;387:22–40.

Ohtori S, Inoue G, Mannoji C, Saisu T, Takahashi K, Mitsuhashi S, Wada Y, Takahashi K, Yamagata M, Moriya H. Shock wave application to rat skin induces degeneration and reinnervation of sensory nerve fibers. Neurosci Lett 2001;315:57–60.

Pang SS, Goldsmith W. Momentum and energy processes during jackhammer operation. Rock Mech Rock Eng 2005;22(3):205–229.

Szabo T. Diagnostic ultrasound imaging: Inside out. Burlington, MA: Elsevier, 2004.

Takahashi N, Wada Y, Ohtori S, Saisu T, Moriya H. Application of shock waves to rat skin decreases calcitonin gene-related peptide immunoreactivity in dorsal root ganglion neurons. Auto Neurosci 2003;107:81–84.

Wang C, Huang H, Pai C. Shock wave enhances neovascularization at the tendon-bone junction. J Foot Ankle Surg 2002;41:16–22.

Wang C, Wang F, Yang K, Huang C, Hsu C, Yang L. Shock wave therapy induces neovascularization at the tendon-bone junction. A study in rabbits. J Orthop Res 2003;21:984–989.